Journal of Applied Physics

RESEARCH ARTICLE | NOVEMBER 04 2019

Atomic origin of Ti-deficient dislocation in $SrTiO_3$ bicrystals and their electronic structures

Xujing Li; Shulin Chen; Mingqiang Li; Kaihui Liu; Xuedong Bai ✉; Peng Gao ✉

Journal of Applied Physics 126, 174106 (2019)
https://doi.org/10.1063/1.5117215

Journal of Applied Physics ARTICLE scitation.org/journal/jap

Atomic origin of Ti-deficient dislocation in $SrTiO_3$ bicrystals and their electronic structures

Cite as: J. Appl. Phys. **126**, 174106 (2019); doi: 10.1063/1.5117215
Submitted: 29 June 2019 · Accepted: 21 October 2019 ·
Published Online: 4 November 2019

Xujing Li,[1,2] Shulin Chen,[2,3] Mingqiang Li,[2] Kaihui Liu,[4,5] Xuedong Bai,[1,a)] and Peng Gao[2,5,6,a)]

AFFILIATIONS

[1]Beijing National Laboratory for Condensed Matter Physics and Institute of Physics, Chinese Academy of Sciences, Beijing 100190, China
[2]Electron Microscopy Laboratory, School of Physics, Peking University, Beijing 100871, China
[3]State Key Laboratory of Advanced Welding and Joining, Harbin Institute of Technology, Harbin 150001, China
[4]State Key Laboratory for Mesoscopic Physics, School of Physics, Peking University, Beijing 100871, China
[5]Collaborative Innovation Centre of Quantum Matter, Beijing 100871, China
[6]International Center for Quantum Materials, Peking University, Beijing 100871, China

[a)]**Authors to whom correspondence should be addressed:** p-gao@pku.edu.cn and xdbai@iphy.ac.cn

ABSTRACT

Dislocations in perovskite oxides have important impacts on their physical and chemical properties, which are determined by their unique atomic environments. In the present study, the structure of dislocations in a 10° low-angle grain boundary of $SrTiO_3$ that was fabricated in an N_2 annealing atmosphere is characterized by spherical aberration-corrected scanning transmission electron microscopy and spectroscopy. We find that the dislocation cores are deficient in titanium (Ti) due to Sr substitution and under Ti occupancy. This differs from previously reported dislocation cores fabricated in an air annealing atmosphere, which show Ti enrichment. The presence of oxygen vacancies and partially reduced Ti are also detected in these Ti-deficient dislocation cores. These findings indicate that atomic structures of dislocations can be very different even when they have the same Burgers vectors. Controllable element segregation in the dislocations and grain boundaries via bicrystal engineering should be very useful for designing devices with novel functions.

I. INTRODUCTION

Dislocations, which are ubiquitous in crystal materials and devices, can be manipulated to produce peculiar physical and chemical properties,[1–3] including unique electronic and ionic transportation behavior,[4,5] switchable resistance,[6,7] ferroelectric polarization suppression and ferroelectric domain wall pinning,[8,9] enhanced current densities in superconducting conductors,[10,11] and low-field magnetoresistance in magnetic films.[12] Therefore, it is of great importance to precisely determine the atomic structures of crystals and to subsequently control the properties of dislocations. Because low-angle bicrystal structures with grain boundaries (GBs) tend to feature regulable and periodic dislocation arrays, bicrystal engineering provides a very useful way to design dislocations with controllable structures and properties (by, e.g., changing tilt angles or via element doping). Many efforts have been made to fabricate bicrystals and reveal their physical and chemical properties.[13–19] Among them, $SrTiO_3$ (STO) bicrystals have been studied extensively as a model system for perovskites.[20,21] Generally, STO bicrystals are fabricated via heat treatment under a uniaxial load in air.[22,23] Under these conditions, the dislocation cores in the GB plane are usually rich in Ti.[22,24] Such Ti-rich cores, which lead to positively charged dislocations, can explain many interesting physical phenomena associated with the electrical activities of electroceramic STOs, such as the presence of a space charge layer[25] and enhanced ionic conductivities.[26,27] Ti enrichment is believed to originate from the generation of Sr vacancies at high temperature and tensional stress at the dislocation cores, which induce a transition in which TiO_6 octahedrons change from corner sharing to edge sharing,[23,28,29] forming a localized Ti-O rock salt phase. However, such a model may be not applicable to all STO dislocations because the atomic structure and chemistry of different dislocations may significantly rely on the history of sample treatment.

In this work, we demonstrate that STO dislocation cores in low-angle bicrystals can be made to be deficient, rather than rich, in Ti by controlling the fabrication conditions. Such Ti-deficient dislocations are obtained by diffusion bonding of two $SrTiO_3$ single crystals at 1000 °C for 10 h in an N_2 atmosphere under uniaxial stress of 2 MPa. The bicrystal structure is characterized by spherical aberration-corrected scanning transmission electron microscopy (Cs-STEM) and spectroscopy. We find that the GB consists of two alternative dislocations labeled A (Ti-O plane terminated) and B (Sr-O plane terminated), which have the same Burgers vector but different atomic arrangements and chemistry. Based on quantitative analyses of energy dispersive X-ray spectroscopy (EDS) results, the ratio of Sr to Ti was estimated to be 0.85:0.70 for dislocation core A and 0.88:0.65 for core B (whereas that of a bulk STO perovskite is 1:1). Also, in the cores, Ti was partially reduced from Ti^{4+} to Ti^{3+} due to the presence of oxygen vacancies, which should lead to different electronic properties and electrical activities.

II. EXPERIMENTAL METHODS

A. Bicrystal fabrication

STO bicrystal with a [001]/(110) 10° tilt GB was fabricated by thermal diffusion bonding of two SrTiO3 single crystals at 1000 °C for 10 h in an N_2 atmosphere, under uniaxial stress of 2 MPa.

B. TEM sample preparation

Thin foils for STEM observations were prepared by a conventional method that includes mechanical polishing and

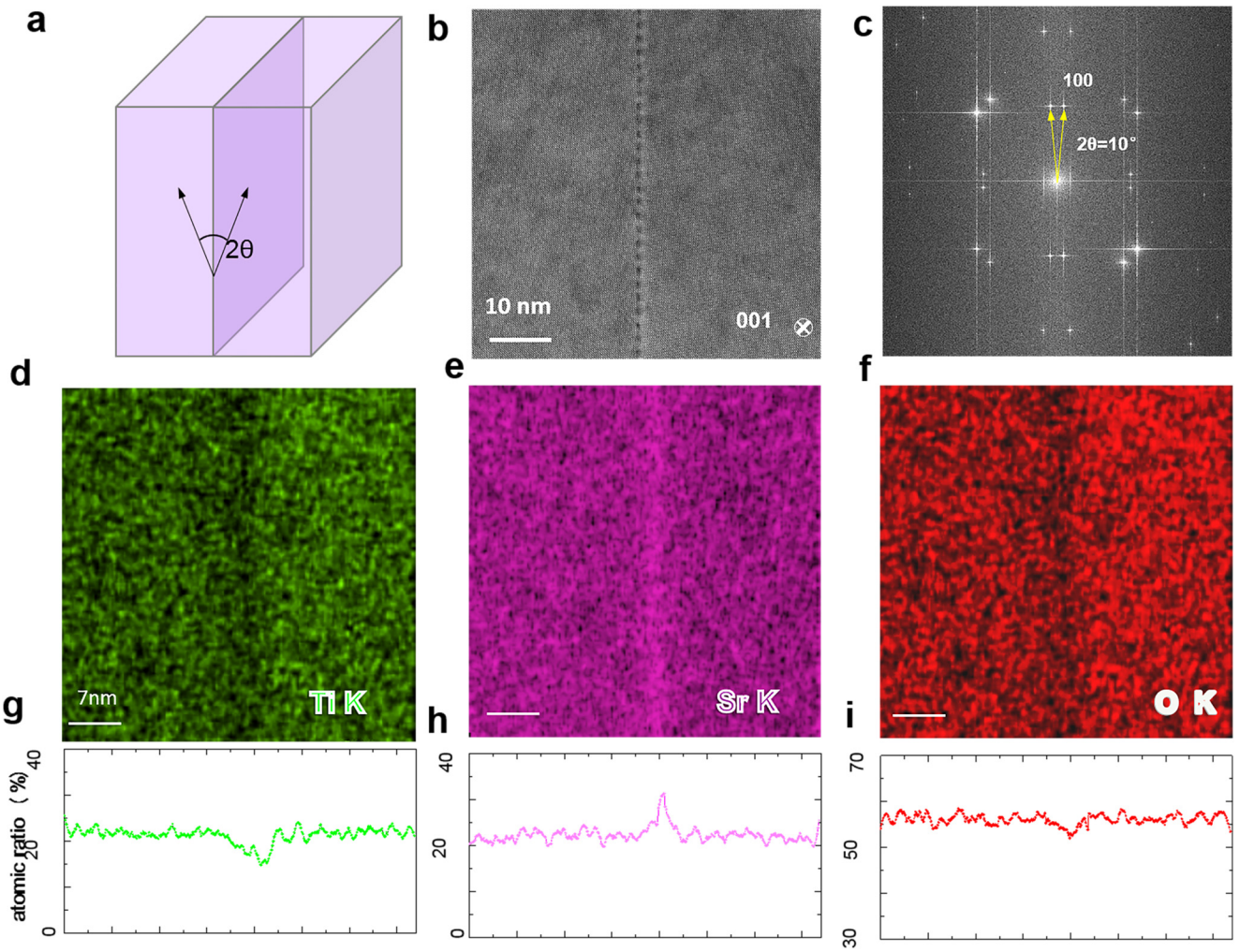

FIG. 1. STO bicrystal fabrication and EDS analysis. (a) The schematic of STO bicrystal with a tilt angle of 10°. (b) HAADF-STEM image and (c) the corresponding fast Fourier transform (FFT) pattern and two yellow arrows confirming the tilt angle of 10°. EDS concentration maps for (d) Ti, (e) Sr, and (f) O and the corresponding line profiles are shown in (g), (h), and (i), respectively.

argon-ion-beam milling. The ion-beam milling was carried out using PIPS™ (Model 691, Gatan, Inc.) with the acceleration voltage of 3.5 kV until a hole was observed. Finally, low-voltage milling was carried out with the acceleration voltage of 0.5 kV to reduce the thickness of the irradiation-damaged layers.

C. STEM observation and EDS analysis

High-angle annular dark field (HAADF) images were recorded at 300 kV using an aberration-corrected FEI Titan Themis G2 with a spatial resolution up to ~60 pm. The convergence semiangle for imaging is 15 mrad, and the collection semiangles'

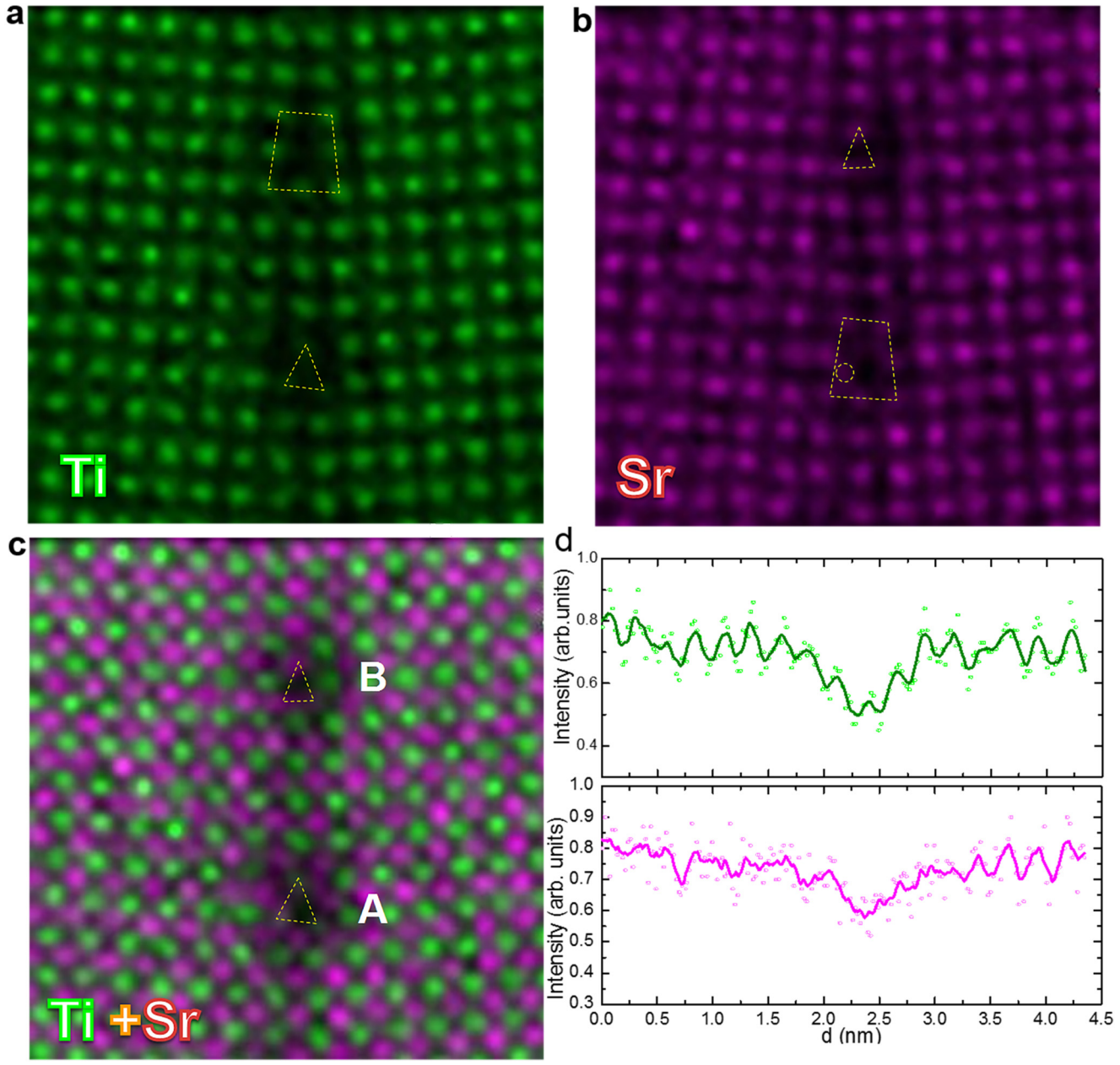

FIG. 2. The atomically resolved EDS maps around the dislocations. (a) Net count map of Ti. (b) Net count map of Sr. (c) Intermix of Sr and Ti. (d) Line profiles of Ti and Sr across the dislocation cores. The yellow dashed quadrilateral and triangle show the dislocation cores A and B, and the dashed yellow circle points to a Sr column appeared at the position of the Ti column.

snap is 48–200 mrad. During imaging, the low electron doses were applied by using small aperture, small beam current, and short scanning time. Typical HAADF images are shown in Fig. 1(b). To determine the occupancy of individual atomic columns in the dislocation cores, the intensity ratio of each atomic column in the cores to that in the bulk was calculated. We used the relation $I^{0.5}$ for HAADF images to estimate the occupancy, where I is the normalized intensity of the atomic columns in the dislocation cores. The EDS experiments were carried out at 300 kV. In order to precisely obtain the elemental information of GB, the EDS data were recorded with the sample being tilt about 15° from the zone axis and maintaining the interface edge-on condition to minimize the channeling effect. Typical net count EDS maps for Sr, Ti, and O are shown in Fig. S1 in the supplementary material. To obtain the atomic percentage of Sr and Ti, the quantitative map (Qmap) was conducted by using the Cliff-Lorimer method. The EDS concentration maps are shown in Fig. 1. The atomic resolved EDS maps of Sr and Ti are obtained on zone axis, which are shown in Fig. 2 and Fig. S2 in the supplementary material. To estimate the average elements' occupancy, linear approximation was applied.

D. Electron energy loss spectroscopy (EELS) analysis

Electron energy loss spectroscopy (EELS) experiments were carried out at 300 kV. The electron beam was slightly spread, and the acquisition time is 0.5 s/pixel. Spectra of line scan from 400 to 490 eV are obtained with an energy dispersion of 0.025 eV, and EELS mapping with a region of ~7 × 3.5 nm^2 from 350 to 860 eV is obtained with an energy dispersion of 0.1 eV, shown in Fig. 4 and Fig. S3 in the supplementary material. The chemical valence of Ti is obtained from the ratio of Ti^{3+} and Ti^{4+} by multiple linear least squares (MLLS) fitting and quantification with Digital Microscopy software (Gatan).

III. RESULTS AND DISCUSSION

Figure 1 shows the schematic of an STO bicrystal with a tilt angle of 10°, along with high-angle annular dark field (HAADF) images recorded in scanning transmission electron microscopy (STEM) mode and the corresponding fast Fourier transform (FFT) pattern. As shown in Fig. 1(b), the misorientation between the two single crystals leads to the formation of an array of dislocations. The FFT in Fig. 1(c) shows two diffraction spots (100) rotated against each other by approximately 10°, which coincides with the designed tilt angle of 10°. The distance between two adjacent dislocation cores is about 2.4 nm, which is in good agreement with the distance (2.2 nm) calculated by Frank's formula,[30]

$$d_{th} = \frac{|b|}{2\sin(\theta/2)},$$

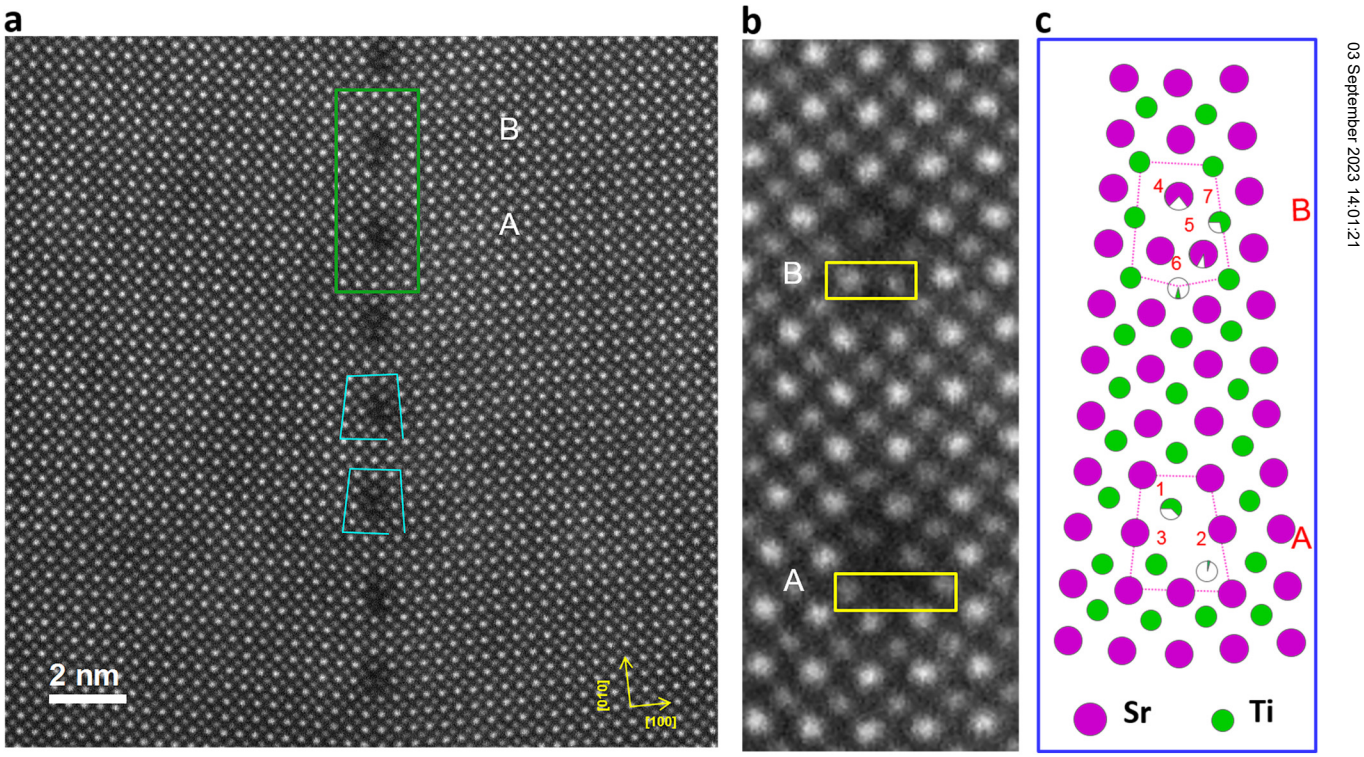

FIG. 3. Atomic structure of the dislocations. (a) Atomic-resolution HAADF-STEM image with the Burgers circuits marked by blue lines, the green rectangle marked location is shown in (b) and the yellow rectangles indicate the termination plane. (c) Schematic for core-structure, and the dashed pink polygons show the dislocation cores with the sector indicating the possible occupancy.

where θ is the tilt angle ($\theta = 10°$) and $|b|$ is the modulus of the Burgers vector (0.3905 nm). To explore the distribution of local elements in the vicinity of the GB, STEM-EDS was carried out. To minimize the channeling effect, the sample was tilted about 15° from the zone axis[31] to record the EDS data for quantitative analyses. The raw EDS count maps for Ti K lines, Sr K lines, and O K lines are shown in Fig. S1 in the supplementary material. At the GB, the net counts for Ti, Sr, and O are reduced with a dark color compared with that in the bulk. The relative changes in the concentrations of Sr, Ti, and O around the GB were also extracted, and their corresponding line profiles across the GB are presented in Figs. 1(d)–1(i). The atomic ratios of each element were calculated by the Cliff-Lorimer method.[32,33] Near the GB, the concentration of Ti decreased while Sr increased, leading to the Ti-deficient dislocation cores at the GB, which is different from previous work.[28] Meanwhile, the concentration of O was lower near the boundary.

Next, atomically resolved EDS maps of Sr and Ti were produced to estimate the compositions of dislocations. The raw maps are shown in Fig. S2 in the supplementary material. To minimize spatial fluctuation, the images were averaged from 10 pairs of

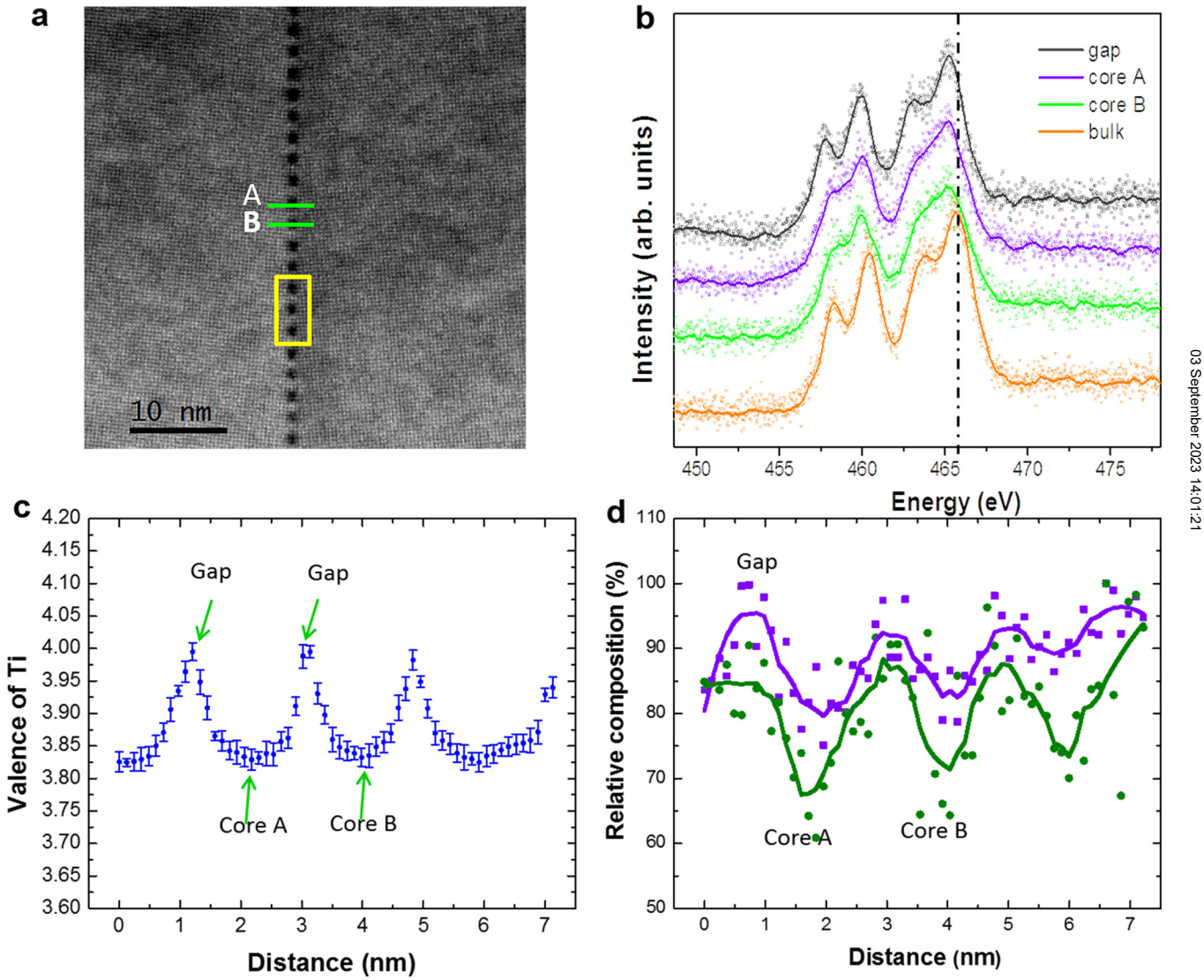

FIG. 4. EELS analysis. (a) The HAADF image with the position of EELS mapping (yellow rectangle). (b) EEL spectra of core A, core B, gap between core A and core B, and bulk aside the boundary. (c) The chemical valence of Ti obtained from EELS mapping results from multiple linear least squares (MLLS) fitting, and the peak and valley correspond to gap and dislocation core, respectively. (d) Intensity distribution of Ti (purple) and O (green) from EELS mapping.

dislocation cores. As shown in Fig. 2, two types of dislocation cores (A and B) appeared at the GB. At each one, the brightness of Ti and Sr columns are very faint, possibly due to the low occupancy. In addition, Sr atoms partly occupy the position of Ti columns. According to the line profile across the GB, although the net counts of Ti and Sr along the boundary are lower compared to bulk regions, the net counts of Ti are reduced much more than that of Sr. To estimate the average element occupancy, linear approximation was applied,[34] which gives a reasonable estimation of local compositions based on EDS analysis.[23] The ratio of Sr to Ti is 1:1 in a bulk perovskite. However, they are 0.85:0.70 in dislocation core A and 0.88:0.65 in core B. The atomic-scale estimation of composition further confirms the phenomenon of Ti deficiency at the GB.

Figure 3 shows an atomic-resolution HAADF-STEM image with two different dislocation cores. The two dislocation cores alternatively appear along the GB and have the same Burgers vector ($\mathbf{b} = \mathbf{a}[100]$), which is the same as that for dislocations in the 10° STO GB annealed in air. Because the intensity of atomic columns in HAADF images is approximately proportional to the atomic number, the brighter spots in the image correspond to Sr-Sr columns, whereas the less bright ones are Ti-O columns. The termination plane for dislocation core A is the Ti-O plane, while that for dislocation core B is the Sr-O plane. A schematic of the structure containing core A and core B with the occupancy of individual Sr and Ti atomic columns, also shown in the figure, can help explain the Ti deficiency qualitatively. In the bulk region, the atomic ratio of Sr to Ti is 1:1, as already mentioned. Within the trapezoid regions, the occupancy of Ti columns is significantly decreased while a more subtle reduction occurs for Sr occupancy. For example, for core A, the Ti occupancy of column 1 is estimated to be 62% and that of column 2 is 11%. In contrast, the occupancy of column 3 is about 100%, which may partly result from Sr substitution of Ti, as shown in Fig. 2. For dislocation core B, the Ti occupancy is 17% for column 6 and 71% for column 7, while the Sr occupancy is about 78% and 83% for columns 4 and 5, respectively. As a result, under occupancy of Ti columns and partial substitution by Sr, both contribute to the Ti deficiency in dislocation core regions.

A few different factors may determine the elemental segregation behavior at dislocation cores.[23,28] Theoretical calculations[35] have suggested that both excess SrO (oxygen vacancy V_O and Sr substitution of Ti to form Sr_{Ti}) and excess Ti (oxygen vacancy V_O and Sr substitution of Ti to form Ti_{Sr}) are energetically stable. Previous studies[23,28] have reported Ti-rich dislocation cores partly due to tensile strain, which tends to form a Ti-O rock salt phase with a larger lattice constant. In our study, the dislocation cores were rich in Sr but deficient in Ti and O. In contrast to previous samples fabricated in air, our sample was annealed in N_2 for a long period of time. Therefore, it is likely that these fabrication conditions mainly drove the formation of these unique dislocation cores.

We also determined the electronic structures of Ti by EELS measurement, which is useful for defining the local chemical valence of Ti.[36,37] The representative Ti spectra for core A, core B, the gap between A and B, and the bulk matrix are shown in Fig. 4. Core A and B feature a larger shift to low energy and less peak splitting in the Ti L-edges, corresponding to the low valence of Ti.[28] In the gap, the spectrum is almost the same as that of the bulk, except for a slight shift. The chemical valence of Ti along the GB is shown in Fig. 4(c). At cores, the average chemical valence of Ti decreases to about +3.6, while at the gap, it remains nearly +4. A significant reduction of O intensity is also observed, even more than that of Ti, further evidence that Ti^{3+} exists in the Ti-deficient dislocation cores. Because electronic and ionic transportation properties at the GB strongly depend on atomic structure and chemistry,[4] the Ti-deficient cores at the GB in the STO bicrystal reported herein likely have an important influence on the crystal's transport and other physical properties, which needs further study in the future.

IV. CONCLUSION

We studied the atomic structure and chemistry of dislocation cores in a 10° $SrTiO_3$ bicrystal that was fabricated at high temperature in N_2. Atomic arrangements and elemental occupancies were determined by atomically resolved Z-contrast imaging and EDS measurements. We found that the dislocation cores were deficient in Ti, in contrast with previous studies that have reported Ti richness in such cores. The deficiency was mainly due to the under occupancy of Ti columns and Sr substitution. Moreover, O vacancies and the presence of reduced Ti (from Ti^{4+} to Ti^{3+}) were also confirmed in the dislocation cores. Our findings suggest that the atomic structure and chemistry of dislocations significantly depend on the fabrication process (i.e., heat treatment in N_2 in the present study vs air in previous studies), providing valuable insights into the relationship between the structures and properties of crystal defects. The ability to control the atomic structure and chemistry of dislocations/GBs by changing the bicrystal preparation process also paves the way to the design of specific defects with unique properties.

SUPPLEMENTARY MATERIAL

See the supplementary material for the raw images of net count EDS maps and the representative EELS spectra.

ACKNOWLEDGMENTS

This work was supported by the National Equipment Program of China (Grant No. ZDYZ2015-1), the National Key R&D Program of China (Grant Nos. 2016YFA0300804 and 2016YFA0300903), the Key Area R&D Program of Guangdong Province (Grant No. 2018B010109009), the National Natural Science Foundation of China (NNSFC) (Grant Nos. 51672007, 11974023, and 51421002), the National Program for Thousand Young Talents of China, and the "2011 Program" Peking-Tsinghua-IOP Collaborative Innovation Center of Quantum Matter. The authors also acknowledge the Electron Microscopy Laboratory at the Peking University for the use of Cs corrected electron microscope.

REFERENCES

[1] A. Bourret and J. Desseaux, Nature **272**, 151 (1978).
[2] Y. L. Tang, Y. L. Zhu, Y. Liu, Y. J. Wang, and X. L. Ma, Nat. Commun. **8**, 15994 (2017).
[3] W. Yu, S. Shen, Y. Liu, and W. Han, Acta Mater. **124**, 30 (2017).

[4]R. A. De Souza, J. Fleig, J. Maier, O. Kienzle, Z. L. Zhang, and W. Sigle, M. Rühle, J. Am. Ceram. Soc. **86**, 922 (2003).
[5]R. A. De Souza, J. Fleig, J. Maier, Z. L. Zhang, W. Sigle, and M. Rühle, J. Appl. Phys. **97**, 053502 (2005).
[6]K. Szot, W. Speier, G. Bihlmayer, and R. Waser, Nat. Mater. **5**, 312 (2006).
[7]R. Waser, Microelectron. Eng. **86**, 1925 (2009).
[8]J. Rodriguez, Y. H. Chu, R. Ramesh, and S. V. Kalinin, Appl. Phys. Lett. **93**, 142901 (2008).
[9]C. L. Jia, S. B. Mi, K. Urban, I. Vrejoiu, M. Alexe, and D. Hesse, Phys. Rev. Lett. **102**, 117601 (2009).
[10]M. A. Schofield, M. Beleggia, Y. M. Zhu, K. Guth, and C. Jooss, Phys. Rev. Lett. **92**, 195502 (2004).
[11]R. F. Klie, J. P. Buban, M. Varela, A. Franceschetti, C. Jooss, Y. Zhu, N. D. Browning, S. T. Pantelides, and S. J. Pennycook, Nature **435**, 475 (2005).
[12]N. D. Mathur, G. Burnell, S. P. Isaac, T. J. Jackson, B. S. Teo, J. L. MacManus-Driscoll, L. F. Cohen, J. E. Evetts, and M. G. Blamire, Nature **387**, 266 (1997).
[13]M. Saito, Z. Wang, and Y. Ikuhara, J. Mater. Sci. **49**, 3956 (2014).
[14]H. Yang, P. G. Kotula, Y. Sato, M. Chi, Y. Ikuhara, and N. D. Browning, Mater. Res. Lett. **2**, 16 (2014).
[15]H. Guhl, H. S. Lee, P. Tangney, W. M. C. Foulkes, A. H. Heuer, T. Nakagawa, Y. Ikuhara, and M. W. Finnis, Acta Mater. **99**, 16 (2015).
[16]B. Feng, T. Yokoi, A. Kumamoto, M. Yoshiya, Y. Ikuhara, and N. Shibata, Nat. Commun. **7**, 11079 (2016).
[17]Z. C. Wang, M. Saito, K. P. McKenna, and Y. Ikuhara, Nat. Commun. **5**, 3239 (2014).
[18]J. J. Bean, M. Saito, S. Fukami, H. Sato, S. Ikeda, H. Ohno, Y. Ikuhara, and K. P. McKenna, Sci. Rep. **7**, 45594 (2017).
[19]K. Y. Cheng, L. Zhang, C. Lu, and T. Kiet, Sci. Rep. **6**, 25427 (2016).
[20]S. Y. Choi, S. D. Kim, M. Choi, H. S. Lee, J. Ryu, N. Shibata, T. Mizoguchi, E. Tochigi, T. Yamamoto, S. L. Kang, and Y. Ikuhara, Nano Lett. **15**, 4129 (2015).
[21]H. C. Du, C. L. Jia, L. Houben, V. Metlenko, R. A. De Souza, R. Waser, and J. Mayer, Acta Mater. **89**, 344 (2015).
[22]T. Mizoguchi, Y. Sato, J. P. Buban, K. Matsunaga, T. Yamamoto, and Y. Ikuhara, Appl. Phys. Lett. **87**, 241920 (2005).
[23]P. Gao, R. Ishikawa, B. Feng, A. Kumamoto, N. Shibata, and Y. Ikuhara, Ultramicroscopy **184**, 217 (2018).
[24]Y. Tokuda, S. Kobayashi, T. Ohnishi, T. Mizoguchi, N. Shibata, Y. Ikuhara, and T. Yamamoto, Appl. Phys. Lett. **99**, 033110 (2011).
[25]Y. M. Chiang and T. Takagi, J. Am. Ceram. Soc. **73**, 3278 (1990).
[26]R. Waser, Solid State Ion. **75**, 89 (1995).
[27]K. Szot, G. Bihlmayer, and W. Speier, Solid State Phys. **65**, 353 (2014).
[28]Z. L. Zhang, W. Sigle, and M. Rühle, Phys. Rev. B **66**, 094108 (2002).
[29]K. Takehara, Y. Sato, T. Tohei, N. Shibata, and Y. Ikuhara, J. Mater. Sci. **49**, 3962 (2014).
[30]F. C. Frank, Philos. Mag. **42**, 809 (1951).
[31]B. Feng, N. R. Lugg, A. Kumamoto, Y. Ikuhara, and N. Shibata, ACS Nano **11**, 11376 (2017).
[32]G. Cliff and G. W. Lorimer, J. Microsc. **103**, 203 (1975).
[33]G. W. Lorimer, Mineral. Mag. **51**, 49 (1987).
[34]Z. Chen, D. J. Taplin, M. Weyland, L. J. Allen, and S. D. Findlay, Ultramicroscopy **176**, 52 (2017).
[35]B. Liu, V. R. Cooper, H. X. Xu, H. Y. Xiao, Y. W. Zhang, and W. J. Weber, Phys. Chem. Chem. Phys. **16**, 15590 (2014).
[36]G. Z. Zhu, G. Radtke, and G. A. Botton, Nature **490**, 384 (2012).
[37]D. A. Muller, N. Nakagawa, A. Ohtomo, J. L. Grazul, and H. Y. Hwang, Nature **430**, 657 (2004).